Computers and Concrete, *Vol. 25, No. 1 (2020) 1-14*
DOI: https://doi.org/10.12989/cac.2020.25.1.001

GS-MARS method for predicting the ultimate load-carrying capacity of rectangular CFST columns under eccentric loading

Nguyen-Vu Luat[1a], Jaehong Lee[1b], Do Hyung Lee[2b] and Kihak Lee[*1]

[1]*Department of Architectural Engineering, Sejong University, 209 Neungdong-ro, Gwangjin-gu, Seoul 05006, South Korea*
[2]*Department of Civil Environmental and Railroad Engineering, Paichai University, 155-40 Baejae-ro, Seo-Gu, Daejeon 35345, South Korea*

(*Received September 23, 2019, Revised December 16, 2019, Accepted December 20, 2019*)

Abstract. This study presents applications of the multivariate adaptive regression splines (MARS) method for predicting the ultimate loading carrying capacity (N_u) of rectangular concrete-filled steel tubular (CFST) columns subjected to eccentric loading. A database containing 141 experimental data was collected from available literature to develop the MARS model with a total of seven variables that covered various geometrical and material properties including the width of rectangular steel tube (B), the depth of rectangular steel tube (H), the wall thickness of steel tube (t), the length of column (L), cylinder compressive strength of concrete (f'_c), yield strength of steel (f_y), and the load eccentricity (e). The proposed model is a combination of the MARS algorithm and the grid search cross-validation technique (abbreviated here as GS-MARS) in order to determine MARS' parameters. A new explicit formulation was derived from MARS for the mentioned input variables. The GS-MARS estimation accuracy was compared with four available mathematical methods presented in the current design codes, including AISC, ACI-318, AS, and Eurocode 4. The results in terms of criteria indices indicated that the MARS model was much better than the available formulae.

Keywords: concrete-filled steel tube; multivariate adaptive regression spline; eccentric loading; ultimate load-carrying capacity; CFST column; MARS

1. Introduction

Concrete-filled steel tubular (CFST) columns are a type of composite structure, made of hollow steel tubes filled with concrete. These steel tubes can be of various cross-sections: circular hollow sections (CHS), square hollow sections (SHS), and rectangular hollow sections (RHS). The CFST column system has mechanical advantages over either reinforced concrete or pure steel members due to the confining effect of the surrounding steel which provides increased strength and greatly improves the ductility of normal concrete. Moreover, the steel tube acts as a permanent formwork that leads to reduced construction time, thus additional cost-saving. As a result, the use of CFST columns has recently expanded throughout the world. Their applications in a variety of civil engineering structures include high-rise buildings, subway platforms, bridges (Zeghiche and Chaoui 2005, Lu and Zhao 2010, Han *et al.* 2014), etc.

Numerous studies on CFST columns have been conducted over the past five decades (Knowles and Park 1969, 1970, Tomii *et al.* 1977, Shakir-Khalil and Zeghiche 1989, Schneider 1998). Reviewing the available literature indicates that the behavior and carrying capacity of CFST columns are governed by their mechanical and geometrical properties. The critical mechanical properties are the strength of the steel and concrete, load eccentricity, and the level of concrete confinement (Neogi *et al.* 1969, Rangan and Joyce 1992, Portolés *et al.* 2011). On the other hand, the principal geometrical parameters are the column slenderness, section slenderness, shape of the hollow cross-section, and the initial geometry of columns (Ghasemian and Schmidt 1999, Bradford *et al.* 2002, Uy *et al.* 2011). For slender columns, the overall instability failure mode occurs due to partial compressive yielding of the steel and cracking of the concrete. In contrast, for short column failure, the cause is the compressive yielding of the steel and crushing of the concrete.

The behavior of CFST columns under eccentric axial loading has previously been investigated numerically and experimentally (Rangan and Joyce 1992, Han and Yao 2003, Fujimoto *et al.* 2004, 2008, Lee *et al.* 2011, Bahrami *et al.* 2012, Zhu *et al.* 2012, Han *et al.* 2013, Gupta *et al.* 2015, Liu *et al.* 2015). Han and Yao (2003) tested 35 concrete-filled rectangular hollow section columns and determined that with eccentric loading, the higher the load eccentricity, the bigger the strength loss was. Zeghiche and Chaoui (Zeghiche and Chaoui 2005) also found a good agreement between a decrease of failure loads and increasing eccentricity ratio. However, to date no simplified models have been proposed, similar to those proposed for the concentrically loaded case, which takes into account the effect of eccentric loading, even in current design codes.

In recent decades, with the rapid development of artificial intelligence techniques, machine learning models

*Corresponding author, Professor
E-mail: kihaklee@sejong.ac.kr
[a]Ph.D. Student
[b]Professor

ISSN: 1598-8198 (Print), 1598-818X (Online)

Table 1 Summary of design codes and their limitations

No.	Design code	Ultimate strength (N_u)	Limitations
1	ACI 318R (2014, 2011, 2008) and AS (AS4100 2012, AS3600 2001)	$N_0 = 0.85 f_c^{'} A_c + f_y A_s$; $N_u = 0.85 N_0$	$B/t \le \sqrt{3E_s/f_y}$; $f_c^{'} \ge 17.2MPa$
2	AS 5100.6 (2004)	$N_u = \phi f_c^{'} A_c + \phi_c f_y A_s$; $\phi = 0.9; \phi_c = 0.6$	$B/t \le 35\sqrt{250/f_y}$; $230 \le f_y \le 400MPa$; $25 \le f_c^{'} \le 65MPa$
3	AISC 360 (2016, 2010)	$N_u = 0.75 N_n$	$B/t \le 2.26\sqrt{E_s/f_y}$; $f_y \le 525MPa$; $21 \le f_c^{'} \le 70MPa$
4	Eurocode 4 (2004)	$N_u = f_y A_s + 0.85 f_c^{'} A_c$ $N_n = \begin{cases} N_0\left[0.658^{N_0/N_{cr}}\right] & (N_0 \le 2.25N_{cr}) \\ 0.877N_{cr} & (N_0 > 2.25N_{cr}) \end{cases}$ $N_0 = f_y A_s + 0.85 f_c^{'} A_c; N_{cr} = \pi^2 (EI_{eff})/(KL^2)$; $EI_{eff} = E_s I_s + C_3 E_c I_c; C_3 = 0.45 + 3\frac{A_s}{A_g} \le 0.9$	$B/t \le 52\sqrt{235/f_y}$; $235 \le f_y \le 460MPa$; $20 \le f_c^{'} \le 60MPa$

(MLMs) have been promoted to solve almost walks of life (Bui *et al.* 2018, Qi and Tang 2018). Due to the prior learning ability, MLMs have already been implemented to predict the strength of structural members. All of them have a common point of using single or hybrid computational intelligent methods. Güneyisi *et al.* (2016) proposed a new formulation for the axial load carrying capacity of circular CFST short columns based on a single gene expression programming (GEP). Ipek and Güneyisi (2019) used the same method for predicting the strength of concrete-filled double skin steel tubular composite columns. Artificial neural networks (ANN) have become the most frequently used method among MLMs. Two conventional ANN models were developed by (Saadoon *et al.* 2012) and (Ahmadi *et al.* 2014) for predicting the ultimate strength of rectangular CFST beam-columns and the capacity of CCFT short columns, respectively. For hybrid computational methods, several models were employed (Bui *et al.* 2018, Ren *et al.* 2019). By fusing a modified firefly algorithm (MFA) with ANN, Bui *et al.* (2018) proposed a novel model, namely MFA-ANN, to predict the compressive and tensile strength of high-performance concrete. Ren *et al.* (2019) developed a new method termed PSVM, by combining support vector machine (SVM) and particle swarm optimization (PSO) in predicting the axial compression of square CFST columns. However, the applied MLMs for the CFST column under eccentric loading are seldom employed.

This study focuses on applying one of the MLMs subsets, Multivariate Adaptive Regression Splines (MARS), on improving the accuracy of predicting the ultimate capacity of rectangular CFST columns under eccentric loading. MARS, which was first proposed by Friedman (1991), is capable of fitting nonlinear, complex relationships between a set of predictors and dependent variables. The space of these predictors is divided into multiple knots in order to fit a spline function between these knots. Some of the main advantages of MARS are the ability to capture the complicated data mapping in high-dimensional patterns and to produce more straightforward, more accurate and faster simulations, and easier-to-elucidate models for both classification and regression problems (Friedman 1991). Some previous applications of MARS in structural engineering include predicting the compressive strength of concrete (Dutta *et al.* 2018), estimating shear strength in reinforced concrete beams(Cheng and Cao 2014), and modeling nonlinear structural interactions (Zhang and Goh 2015). Nonetheless, predictive models derived from the MARS algorithm have never been implemented for CFST problems.

Fused MARS with grid search (GS) method, this paper presents a new model, namely GS-MARS, was developed to predict the ultimate capacity of eccentric loaded CFST columns concerning the width of rectangular steel tube (*B*), the depth of rectangular steel tube (*D*), load eccentricity (*e*), length of column (*L*), wall thickness of the steel tube (*t*), the cylinder compressive strength of concrete ($f_c^{'}$), and the yield strength of steel (f_y). In which, the GS method was utilized for optimizing MARS' hyperparameters. The proposed MARS model is expressed by an explicit formulation in terms of the variables mentioned above and was then compared against available design codes.

2. Overview of available studies and current design codes for CFST columns

Because of the great advantages composite members provide, including high strength, good ductility, high energy absorption capacity, and saving construction time, CFST members and structures have been widely investigated. This research has led to the development of many design codes in several countries, such as American codes ACI-318 and AISC360, Eurocode 4, and Australian Standard AS5100.6, etc. For design purposes, all of these codes provide formulae and some limitations on material strength and section slenderness, as given in Table 1. Tao *et al*. (2008) who evaluated the applicability of AISC and Eurocode 4 for 445 rectangular and 448 circular CFST stub columns, indicated that Eurocode 4 provided better strength predictions than the others for circular CFST stub columns, but AISC was better for rectangular CFST stub columns on the other hand. When comparing design calculations with test results, Aslani *et al.* (2015) pointed out that the AS, ACI, and Eurocode 4 models provided a better prediction of ultimate strength for short rectangular CFST columns compared with the other models.

It should be noted that, outside the limitations, these codes might give less accurate value estimations (Aslani *et al.* 2015). In addition, although within the limitations, the ultimate strength predictions from these design codes show significant divergence from experimental results. Therefore, to increase prediction accuracy, some proposed models might provide further improvement. (Tao *et al.* 2008, Kuranovas *et al.* 2009, Güneyisi *et al.* 2016).

3. Multivariate Adaptive Regression Splines (MARS)

Multivariate adaptive regression splines method was first introduced by Friedman (1991), as a procedure for adaptive nonlinear and nonparametric regression that makes no assumption about the underlying functional relationship between the predictors and the target outputs. The general expression of nonparametric regression can be represented as

$$y_i = f(x_{i1}, x_{i2}, \ldots x_{ij}) + \varepsilon_i = f(\mathrm{X}) + \varepsilon_i \qquad (1)$$

in which $\mathbf{X}=(x_{i1}, x_{i2},\ldots,x_{ij})$ is an $i\times j$ matrix of j input features and i samples and ε_i is the error distribution of the i^{th} sample, also called noise. The main goal of this regression is to estimate the general function of high dimensional arguments $f(x_{i1}, x_{i1}, \ldots x_{ij})$ directly, rather than to estimate parameters. For this purpose, it is assumed that $f(X)$ is a smooth, continuous function.

A MARS model is established by applying basis functions (known as terms) to approximate the function $f(X)$. Basis functions are splines (also called smooth polynomials) which have pieces including piece-wise linear and piece-wise cubic functions that connect smoothly together. However, only the piece-wise linear function is expressed for simplicity. The interface points between the linear piece-wises are called knots, denoted t. The knot location separates the spline basis function (Fig. 1) into two-sided truncated functions, is expressed formally as

$$b_q^-(x-t) = \left[-(x-t)\right]_+^q = \begin{cases} (t-x)^q & \text{if x } < \text{ t} \\ 0 & \text{otherwise} \end{cases} \qquad (2)$$

$$b_q^+(x-t) = \left[+(x-t)\right]_+^q = \begin{cases} (x-t)^q & \text{if x } > \text{ t} \\ 0 & \text{otherwise} \end{cases} \qquad (3)$$

where t is the knot location, $b_q^-(x-t)$ and $b_q^+(x-t)$ are the spline functions, the $[]^+$ ensures these values are positive, and the power q equals to 1 for simplicity as

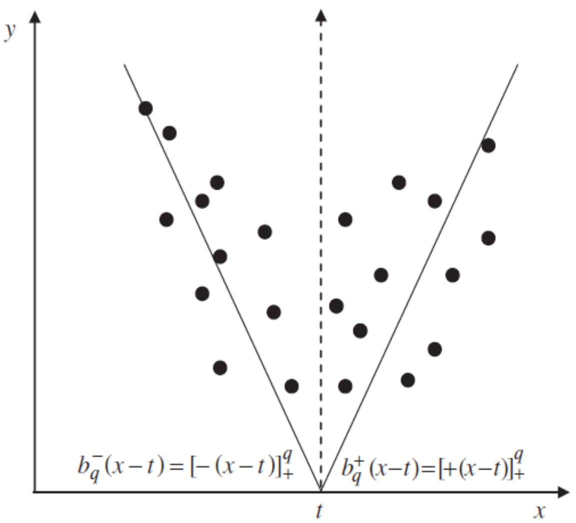

Fig. 1 The basis function and knot

mentioned above.

The general form of the MARS model for predicting output can be expressed as

$$\hat{y} = f(X) = c_0 + \sum_{m=1}^{M} c_m B_m(x) \qquad (4)$$

where x is the input variable; c_0 is a constant; $B_m(x)$ is the m^{th} basis function; and c_m is the coefficient of $B_m(x)$.

In general, MARS contains the following three steps: (i) the constructive phase: a forward stepwise algorithm to select certain spline basis functions, (ii) the pruning phase: a backward stepwise algorithm to delete unnecessary basis functions until the "best" set is found, and (iii) optimum model selection. The constructive phase first starts on the training data with only the intercept, c_0, then several knots are created automatically. These knots are points at random locations within the range of each input variables to define a pair of basis functions. At each step, the model adopts the knot and its corresponding pair of basis function that produces the largest decrease in the residual sum of squares error. Considering a current model with a number of basis functions (M), the next pairs are added to the model in the form

$$c_{m+1} B_m(X)\left[+(x_j - t)\right]_+^q + c_{m+2} B_m(X)\left[-(x_j - t)\right]_+^q \qquad (5)$$

This process continues until the maximum number of terms M_{max} is reached. The value for M_{max} should be chosen larger than the optimal model size as referenced in (Friedman 1991). Typically, the basis functions addition leads to a very complicated and overfit model.

In the second phase, a backward deletion is employed to overcome this problem. The aim of this phase is to find an optimal model by removing redundant basis functions and irrelevant variables as well. Friedman (1991) also recommended the generalized cross-validation (*GCV*) originally proposed by Craven and Wahba (1978) as deletion criterion. The value of *GCV* is defined as follows

$$GCV(M) = \frac{1}{n} \times \frac{\sum_{m=1}^{M}(y_i - \hat{y}_i)}{\left(1 - {C(M)}/{n}\right)^2} \qquad (6)$$

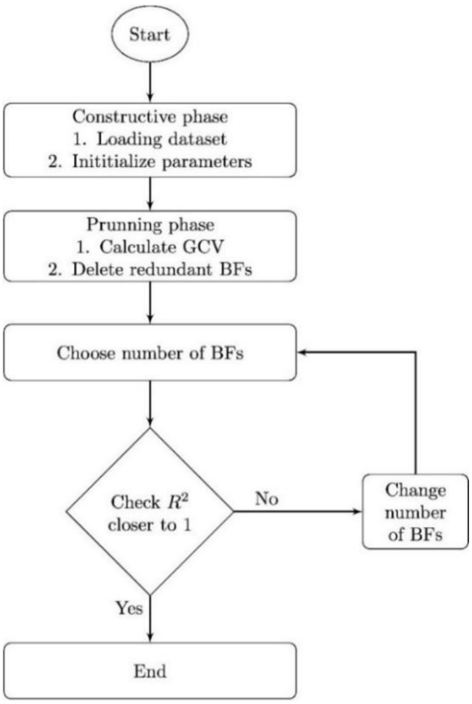

Fig. 2 The flowchart of the MARS model

where n is the number of data sets, y_i is the response value of the i^{th} data, $\hat{y}_i$ is the predicted values obtained from the MARS model of the i^{th} data, and $C(M)$ is a penalty factor that increases with the number of terms that can be determined as

$$C(M) = M + dM \tag{7}$$

where d is a cost penalty factor for each basis function optimization and is a smoothing parameter. Friedman (1991) provides more details about the selection of d. At each backward step, a basis function is removed to minimize Eq. (6), until an adequately fitting model is found. Finally, in the third phase, the best MARS model is selected. Fig. 2 shows the MARS model flowchart.

An analysis of variance (ANOVA) decomposition of the MARS model can be used to assess the contributions from the input variables and the basis functions. This procedure groups together all the basis functions that involve one variable and another grouping of terms that involve pairwise interactions. ANOVA function for MARS model is given by the following expression

$$f(x) = \beta_0 + \sum_{B=1} f_i x_i + \sum_{B=2} f_{ij} x_{ij} + \sum_{B=3} f_{ijk} x_{ijk} + ... \tag{8}$$

where $\sum_{B=1} f_i x_i$ is the total basis functions that involve only a single variable, $\sum_{B=2} f_{ij} x_{ij}$ is total basis functions that involve exactly two variables, and $\sum_{B=3} f_{ijk} x_{ijk}$ represents the contributions from three variables interactions (if present).

4. Description of the experimental database

The experimental data used in this study consists of 141 eccentric loaded rectangular CFST columns as reported by various studies and given in Appendix A. The test configuration taken into account is an eccentrical axial compression test which is illustrated in Fig. 3.

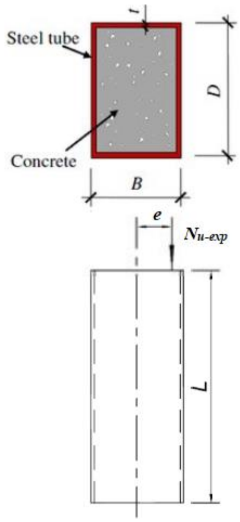

Fig. 3 Square CFST column under eccentric loading

Table 2 Summary of input settings and outputs

Description	Notation	MARS Parameter	Min.	Max.	Mean	Std.
Width of steel tube	B	X_1	65.00	323.00	147.44	53.83
Depth of steel tube	H	X_2	47.30	323.00	166.82	48.15
Thickness of steel tube	t	X_3	2.65	10.01	4.52	1.48
Length of column	L	X_4	360.00	4910.00	1857.72	1111.84
Concrete cylinder strength	f_c'	X_5	15.01	80.30	44.56	20.16
Yield strength of steel	f_y	X_6	254.00	761.00	393.80	145.73
Eccentricity	e	X_7	0.90	300.00	44.56	20.16
Axial strength	N_u	y	232.00	4100.00	1220.28	805.30

The input parameters used to predict the ultimate strength of the rectangular CFST columns consist of the width (B) and depth (H) of the steel tube, the thickness of the steel tube (t), the length of the column (L), the concrete cylinder strength (f'_c), the yield strength of steel (f_y), and eccentricity (e). The test failure load (N_u) is used as the output variable. A summary of input settings and output values is listed in Table 2.

5. Proposed MARS model and application results

5.1 Preprocessing data

Model input and output variables commonly have different dimensions and orders of magnitude. Thus, they need to be normalized to make training less sensitive to the scale of the input variables and to eliminate their dimensions. Moreover, normalization makes the problem better conditioned and prevents numerical difficulties during the calculation. Therefore, all variables are normalized to the range of [0, 1] using the min-max normalization method, which is expressed as follows

$$x_{norm} = \frac{x - \min(x)}{\max(x) - \min(x)} \tag{9}$$

where, x is the original value and x_{norm} is the normalized value.

The K-fold cross-validation method is used in this research to reduce the over-fitting problem in the selected model. For 141 experimental data, the 5-fold was chosen to build the MARS model. Firstly, the whole data was divided into two partitions, namely training set with 120 cases (85%) and testing set with the remaining of 21 cases (15%). To implement the cross-validated procedure, the training data were randomly selected and split into 5 distinct folds, which means each fold contains 24 cases (20% of 120). For each iteration, one of five folds is used for validating while the four remaining folds are used for training the MARS model. This procedure is repeated for each fold in the training set until all folds were used once as the validation fold. With each combination of MARS' hyperparameters, five models would be built and evaluated using some criteria indices. Based on each fold's performance, the optimal model is chosen and tested the testing set again.

5.2 MARS model

The interpreted high-level programming language, Python, with its implementation called *py*-earth package, were used for the development of the MARS model. One may construct a MARS model with a variety of parametric options, including a maximum basis function (max terms) $M_{\max}$, maximum interaction $I_{\max}$, and penalty parameter d. However, while setting the optimal parameters simultaneously is difficult using MARS, such optimization greatly improves the prediction accuracy of MARS. The authors thus utilized GridSearchCV, a tool in the scikit-learn package (Pedregosa *et al.* 2011) to overcome this problem. Scikit-learn is a Python library that contains a set of state-of-the-art machine learning algorithms, which allows non-machine learning experts to apply many well-known machine learning techniques. Moreover, it is able to implement various prediction methods if the estimator used. The estimator parameters used to apply these methods are optimized by a cross-validated grid-search over a parameter grid. The combination of GridSearchCV and the MARS model, which can be abbreviated as the GS-MARS model, is illustrated by the flowchart in Fig. 4.

The performance of the proposed GS-MARS model was evaluated by using the following criteria indices:

• Coefficient of Determination (R^2)

The R^2 is the common measure of determination between the predicted values and actual values and was used as the main criterion to evaluate the performance of the proposed model. The value of R^2 can be determined as follows

$$R^2 = 1 - \frac{\sum_{i=1}^{n}(y_i - \hat{y}_i)^2}{\sum_{i=1}^{n}(y_i - \bar{y}_i)^2} \tag{10}$$

Table 3 The GS-MARS model parameters

Component	Pyearth parameter	Setting
GridSearchCV		
Estimator type	estimator	earth()
Parameter grid	param_grid	{[1], [2], [3], [4], [5]}
Evaluation	scoring	neg_mean_squared_error
Cross-validation	cv	5
Training partition		85%
Validation partition		15%
MARS model		
Maximum number of basis functions [1]	max_term ($M_{\max}$)	(1; 40)
Maximum interaction of terms [2]	max_degree ($I_{\max}$)	(1; 9)
Number of extreme data values of each feature not eligible as knot locations	end_span	-1
Smoothing parameter [3]	penalty (d)	(2; 4)
Parameter controlling end_span [4]	endspan_alpha	(0; 1)
Parameter controlling endspan_alpha [5]	minspan_alpha	(0; 1)
Kind of feature importance	feature_importance _type	GCV

where y is the actual values; $\hat{y}_i$ is the predicted value; $\bar{y}_i$ is the mean of the actual values; and n is the number of samples. For a prediction model with high accuracy, R^2 should be close to 1, which is the maximum value.

• Root Mean Square Error ($RMSE$)

$$RMSE = \sqrt{\frac{1}{n} \times \sum_{i=1}^{n}(y_i - \hat{y}_i)^2} \tag{11}$$

• Mean Absolute Percentage Error ($MAPE$)

$$MAPE = \frac{1}{n} \times \sum_{i=1}^{n} \frac{|y_i - \hat{y}_i|}{y_i} \tag{12}$$

Table 3 lists the parameters for the proposed GS-MARS model. The parameters used in this model are as follows:

• The parameter grid consists of 5 parameters of the MARS model.
• Scoring evaluation is mean square error (MSE) and calculated by: $MSE = \frac{1}{n}\sum_{i=1}^{n}(y_i - \hat{y}_i)^2$
• The training partition size was 85%.
• The size of testing partition was 15%.
• The maximum number of basis function for training is in the range of 1 and 40.
• The maximum interaction of terms is from 1 to 9.
• The number of extreme data values of each feature not eligible as knot locations is a default value of -1.
• The penalizing parameter is in the range of 2 and 4, with a default value of 3.
• The parameter controlling endspan parameter is in the range of 0 to 1.

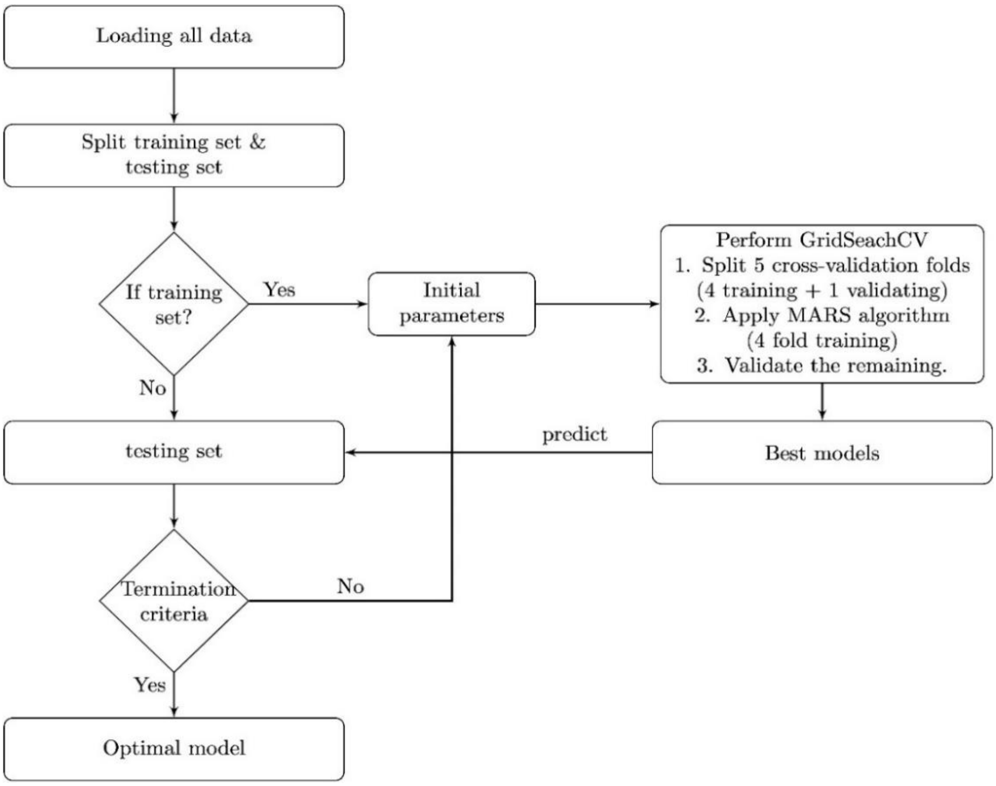

Fig. 4 The flow chart of the GS-MARS model

• The parameter controlling minspan parameter is in the range of 0 to 1.
• The feature importance criteria is GCV.

5.3 GS-MARS performance

This study evaluated the model's performance using the *K*-fold method and a stratified 5-fold cross-validation approach. Random selection divided the 120 of training data into 5 distinct folds. Each fold was employed in turn as validating data, with the remaining folds used as training data, ensuring that all dataset instances were applied in both the training and validating phases.

Table 4 shows the performance of the GS-MARS model in predicting the ultimate compressive strength of CFST columns over 5 folds. As shown in this table, the GS-MARS model attains very good R^2 values for both training set (R^2=0.983) and testing set (R^2=0.968), indicating that the model accurately estimates the underlying function of CFST column compressive strength. The proposed model also yields small average *RMSE* values for training and testing data of 89.72 kN and 124.40 kN compared to the average actual values.

The average of *MAPE* were 8.39% and 8.99% for training and testing prediction, respectively, with both values below 10% indicating the robustness of the GS-MARS model. The small values of standard deviation, illustrating that the proposed MARS model also provides stable prediction, were only 0.73% and 0.87% for training and testing data, respectively.

The key parameter settings of the GS-MARS model are also given in Table 4. Remarkably, the values of the maximum basis function $M_{\max}$ which varied in a range from 21 to 35, affect the accuracy of prediction significantly. In addition, the number of interactions among input variables $I_{\max}$ alternated between 2 and 3.9. It was found that there is no fold that had a default value of penalty parameter d inside the referred range (Friedman 1991). Obviously, choosing suitable parameter values simultaneously is a challenge for users. However, it should be noted that the instances of these parameter values depend on user experience and may be outside the suggested range. This statement is in good agreement with Cheng and Cao's (2014, 2016) investigations.

Table 4 Prediction performance of GS-MARS with 5 K-folds and parameter settings

Fold	Training			Testing			Parameter		
	RMSE (kN)	*MAPE* (%)	R^2	*RMSE* (kN)	*MAPE* (%)	R^2	$M_{\max}$	$I_{\max}$	*d*
1	97.13	8.48	0.9853	113.12	10.01	0.9825	21	3	2.5
2	95.19	8.85	0.9862	125.92	8.58	0.9726	25	3	3.5
3	79.41	7.22	0.9907	96.53	7.73	0.9833	35	2	2
4	85.55	8.28	0.9883	156.80	9.24	0.9661	21	2	2.7
5	91.33	9.10	0.9872	129.61	9.39	0.9685	29	3	3.9
Average	89.72	8.39	0.9875	124.40	8.99	0.9746			
Std.	7.27	0.73	0.0021	22.27	0.87	0.0079			

Fold 2 was selected to derive the formulation of the MARS model since its results are similar to the average values. Table 5 demonstrates the approximation function for predicting fold 2 and presents the related basis functions of the MARS model with the corresponding equations and coefficients (c_m). Clearly, all seven input variables appear in

Table 5 Basis functions of GS-MARS model with corresponding equations and coefficients

$B_m(x)$	Equation	(c_m)	$B_m(x)$	Equation	(c_m)
$B_0(x)$	1	1828.2300	$B_{15}(x)$	$max(0, f_c^{'} - 15) * B_{14}(x)$	-0.0003
$B_1(x)$	$max(0, B - 65)$	6.8469	$B_{16}(x)$	$max(0, e - 37) * B_1(x)$	n/a
$B_2(x)$	$max(0, e - 3.75)$	-11.4375	$B_{17}(x)$	$max(0, 37 - e) * B_1(x)$	0.2553
$B_3(x)$	$max(0, f_y - 618) * B_1(x)$	0.1891	$B_{18}(x)$	$max(0, f_y - 351) * B_{12}(x)$	0.0028
$B_4(x)$	$max(0, 618 - f_y) * B_1(x)$	n/a	$B_{19}(x)$	$max(0, f_c^{'} - 15) * B_2(x)$	-0.0011
$B_5(x)$	$max(0, f_c^{'} - 68.5)$	-52.7446	$B_{20}(x)$	$max(0, f_c^{'} - 65.7) * B_{13}(x)$	0.0282
$B_6(x)$	$max(0, 68.5 - f_c^{'})$	-12.6848	$B_{21}(x)$	$max(0, f_y - 618) * B_2(x)$	-3.2541
$B_7(x)$	$max(0, f_y - 550)$	11.3966	$B_{22}(x)$	$max(0, 618 - f_y) * B_2(x)$	0.0190
$B_8(x)$	$max(0, 550 - f_y)$	-2.0583	$B_{23}(x)$	$max(0, e - 80)$	8.4321
$B_9(x)$	$max(0, H - 210)$	11.7736	$B_{24}(x)$	$max(0, H - 152) * B_8(x)$	n/a
$B_{10}(x)$	$max(0, 210 - H)$	-11.6269	$B_{25}(x)$	$max(0, 152 - H) * B_9(x)$	0.0383
$B_{11}(x)$	$max(0, t - 3)$	91.2767	$B_{26}(x)$	$max(0, 32 - f_c^{'}) * B_{24}(x)$	-0.0036
$B_{12}(x)$	$max(0, L - 2600)$	n/a	$B_{27}(x)$	$max(0, H - 65) * B_{22}(x)$	-9.63e-5
$B_{13}(x)$	$max(0, 2600 - L)$	0.1043	$B_{28}(x)$	$max(0, L - 2600) * B_4(x)$	-2.72e-5
$B_{14}(x)$	$max(0, L - 1800) * B_2(x)$	0.0117	$B_{29}(x)$	$max(0, f_y - 254) * B_6(x)$	-0.0333

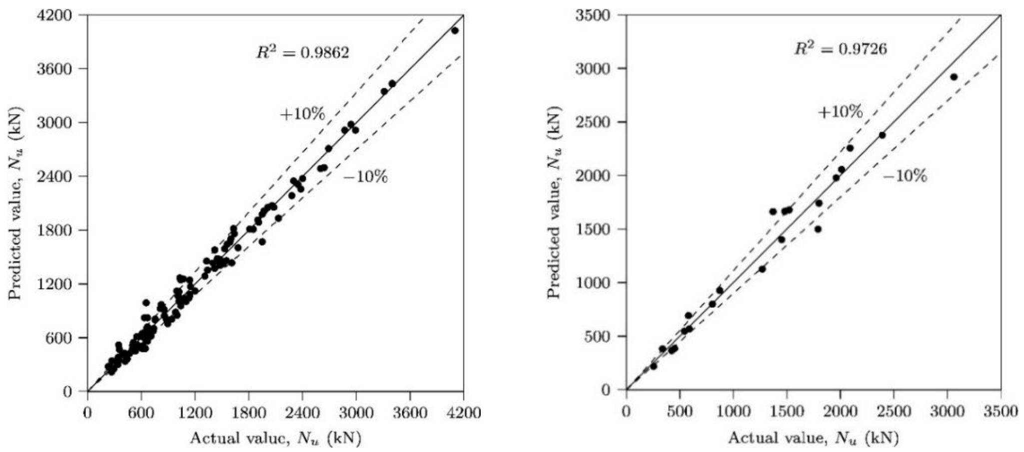

(a) Training set (b) Testing set

Fig. 5 Predicted and actual values for the training and testing sets

the approximate functions. It should be noted that, before training, all input parameters were normalized using Eq.(9). Hence, the basis functions in Table 6 were re-scaled before deriving corresponding equations. Finally, the ultimate axial strength of rectangular CFST columns N_u under eccentric loading was expressed by the MARS model as follows

$$N_u=1828.23+6.84963\times B_1(x)-11.4375\times B_2(x)+0.18914\times B_3(x) -52.7446\times B_5(x)-12.6848\times B_6(x)+11.3966\times B_7(x)-2.05827 \times B_8(x)+11.7736\times B_9(x)-11.6269\times B_{10}(x)+91.2767\times B_{11}(x)+0.10431 \times B_{13}(x)+0.01170\times B_{14}(x)-0.00031\times B_{15}(x)+0.25525\times B_{17}(x) +0.00281\times B_{18}(x)-0.00108\times B_{19}(x)+0.02821\times B_{20}(x)-3.25414 \times B_{21}(x)+0.01898\times B_{22}(x)+8.43210\times B_{23}(x)+0.03832\times B_{25}(x) -0.00358\times B_{26}(x)-9.63\times 10^{-5}\times B_{27}(x)-2.72\times 10^{-5} \times B_{28}(x)-0.03325\times B_{29}(x) \tag{13}$$

Fig. 5 graphically shows the correlation between the predicted value and actual value for fold 2 and the test set. It is clear that most data points in training and testing sets fall within the ±10% line.

Table 6 Results of ANOVA decomposition

Function	GCV	#B_m (x)	Variable (s)	Function	GCV	#B_m (x)	Variable(s)
1	135,431.76	1	B	11	64,062.71	1	L, f_{sy}
2	81,188.71	2	e	12	55,455.81	1	$L, f_c^{'}$
3	99,061.49	2	$f_c^{'}$	13	109,101.61	2	f_{sy},e
4	137,164.20	2	f_{sy}	14	68,866.72	1	H, f_{sy}
5	240,749.67	2	H	15	52,940.60	1	$f_{sy}, f_c^{'}$
6	80,611.93	1	t	16	62,074.53	1	$L, f_c^{'}, e$
7	59,171.08	1	L	17	87,225.34	1	$B, f_c^{'}, e$
8	67,848.67	1	B, f_{sy}	18	77,824.38	1	$H, f_{sy}, f_c^{'}$
9	79,710.32	1	L,e	19	67,020.00	1	H,f_{sy},e
10	134,721.77	1	B,e	20	88,234.45	1	B,L,f_{sy}

As mentioned above, one of the most important advantages of MARS is its capacity to inspect the importance of input variables based on ANOVA

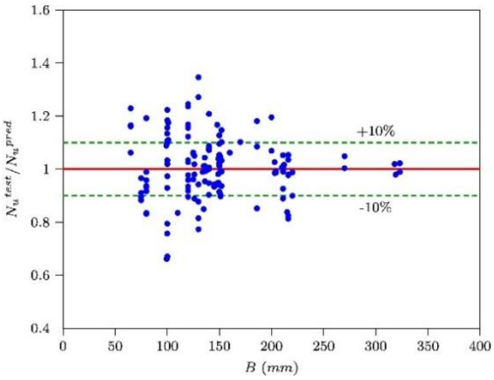

(a) Width of rectangular CFST column

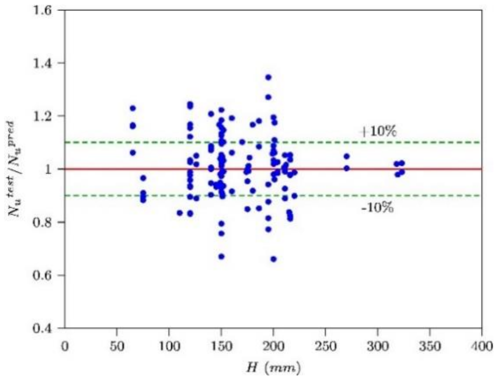

(b) Depth of rectangular CFST column

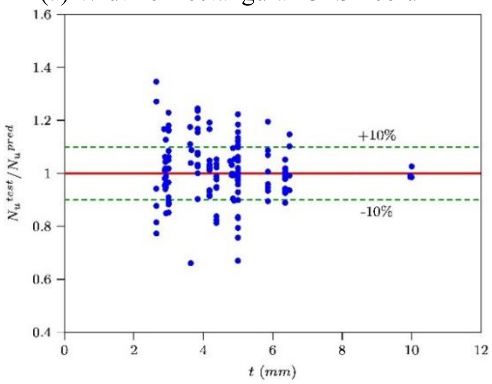

(c) Wall thickness of CFsST column

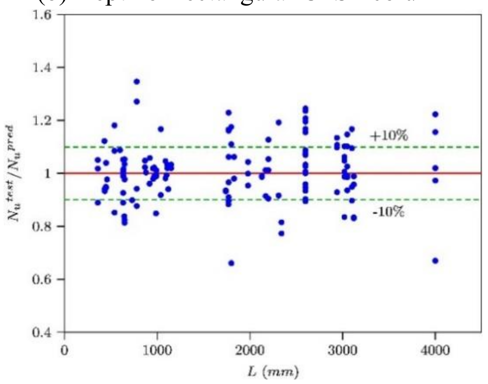

(d) Length of CFST column

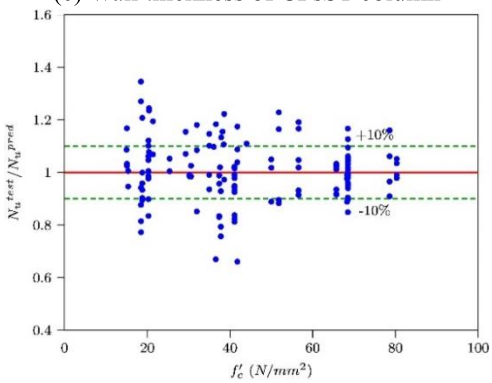

(e) Cylinder compressive concrete strength

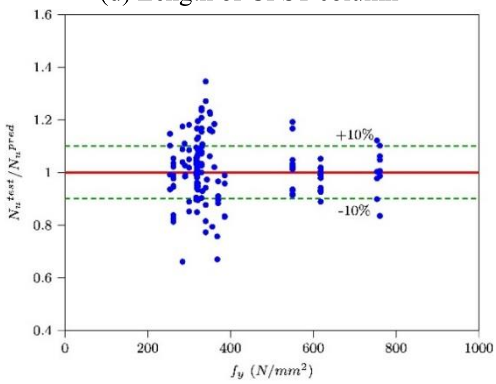

(f) Yield strength of steel tube

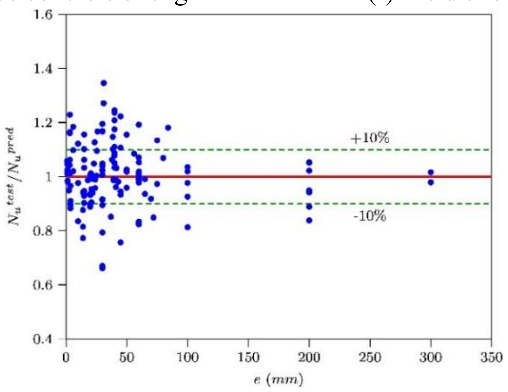

(h) Eccentricity

Fig. 6 Ratio of actual results/predicted results versus input variables

decomposition. Table 6 shows the ANOVA decomposition of the proposed MARS model for fold 2. The GCV column indicates the significance of the corresponding ANOVA functions through the GCV score for a model with all corresponding basis functions to that specific ANOVA function eliminated. This GCV value is employed to evaluate whether the ANOVA function makes a significant contribution to the model or only marginally increases the

Table 7 Comparison of proposed model performance and current design codes

Function	MARS		AISC360 (2016)	ACI318 (2014)	AS5100.4 (2004)	Eurocode 4 (2004)
	Training set	Testing set				
RMSE (kN)	89.72	124.40	785.93	706.47	647.56	1127.88
MAPE (%)	8.39	8.99	40.28	44.94	39.79	78.30
R^2	0.9875	0.9746	0.50	0.52	0.50	0.53

global GCV score. The $\#B_m(x)$ column shows the number of basis functions in the ANOVA function and the variable(s) column gives the particular input features related to the ANOVA function.

The interaction of predictors with the proposed MARS model graphically presents in Fig. 6. The ratio of actual values (N_u^{test}) and predicted values (N_u^{pred}) versus seven predictors respectively are plotted to illustrate their effectiveness. These plots indicated that even though there are accumulations of data at a specific range for each variable, the predicted values have various scatters which perform an overestimate (under the solid red line) or an underestimate (above the solid red line). This proves that the generated MARS model does not depend exactly on any particular variables. Therefore, it can be stated that the used predictors are fairly effective in the proposed model. For further evaluation, Fig. 6 shows that only about 25% data points are outside the margin of ±10% (dashed line). By observing Fig. 6(d) and Fig. 6(e), it is found that the proposed model can be applied extensively for column length less than 3000 mm and the cylinder compressive of concrete in the range of 20 to 80 MPa.

5.4 Results comparison with available models

To demonstrate the comparative performance of the developed MARS model, this study compared results with those obtained by four current design codes including AISC, ACI, AS, and Eurocode 4. Table 7 presents the comparative results with regard to determining *RMSE*, *MAPE*, and R^2. The *RMSE* values for MARS, AISC, ACI, AS5100.4, and Eurocode 4 were, respectively, 107.06, 785.93, 706.47, 647.56, and 1127.88. These results show that MARS is the fittest model in terms of minimizing *RMSE* values, with a value nearly 83% below the second-best model from AS5100.4 in accordance with the testing set. The predictions by Eurocode 4 were the worst model in terms of *RMSE*, returning values more than nine times greater than the MARS model. This tendency is in perfect agreement with the conclusions of Tao *et al.* (2008).

In terms of *MAPE*, the MARS model also yielded the smallest estimation errors for training and testing data, 8.39 and 8.99, respectively. These values were around 31% lower than the second-best model (AS5100.4), which was roughly 40% below the Eurocode 4 performance. Moreover, the MARS model achieved the best results, which were very close to 1, in terms of R^2 for both training and testing data (R^2_{train}=0.9875 and R^2_{test}=0.9746).

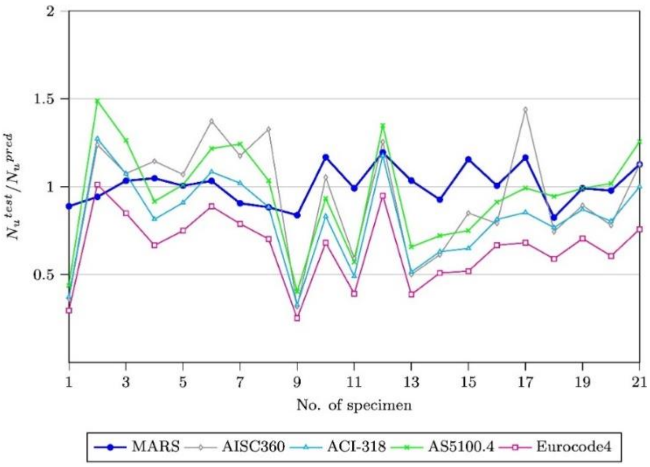

Fig. 7 Actual-to-predict-strength ratio over testing set performance

The predictability performance of these models is presented in Fig. 7 with details of actual value (N_u^{test}) and predicted value (N_u^{pred}) ratio for the testing set. This figure shows that MARS' line connecting ratio points lie closest to the perfect line (N_u^{test}/N_u^{pred} = 1), which means MARS has the ability to generate results that are in closest agreement with the actual results.

6. Conclusions

The aim of this study was to propose a new model with an explicit formulation for predicting the ultimate carrying-capacity (N_u) of rectangular CFST columns. The derived formulation is developed by combining grid search cross-validation technique and the MARS model to determine optimal MARS' parameters. In order to propose the model, a database containing 141 eccentric loaded rectangular CFST columns data sets with a total of seven variables was collected. Based on the discussion above and comparisons of the proposed model with available design codes, some conclusions can be given, as follows:

1. It was found that the MARS model can be efficiently utilized to develop an empirical formulation for predicting the ultimate carrying-capacity of rectangular CFST columns under eccentric loading for various materials and geometrical properties. Moreover, the derived formulation can be employed as a handy prediction tool with satisfactory predictability. However, since its expression is rather cumbersome and complex, it is better to transfer this model to a computer to save time and minimize errors.
2. Constructing a MARS model with various parameter choices is a complicated and challenging process. The three most important parameters must be considered, including the maximum basis function M_{max}, maximum interaction I_{max}, and penalty parameter d. However, the best values may lie outside the recommended ranges.
3. To assess the performance of the MARS model to predict, this study compared MARS against four current design codes, including AISC360, ACI-318, AS5100.4,

and Eurocode 4. The results illustrated MARS' superior estimation capability, providing a coefficient of determination and an actual-to-predicted-value ratio of close to 1, as well as very low values in error terms (*RMSE*, *MAPE*). The code design equations were generally conservative when performing the database in this study, such as Eurocode 4, which tends to overestimate the ultimate load-carrying capacity. This trend can be explained, since some input parameters were outside of the code limitations, and the eccentricity effect was not considered.

4. It should be noted that since the developed GS-MARS model predicts based on the knot values and the basis function, thus interpolation between the knots of input variables are more accurate and reliable than extrapolations. Moreover, the scope of applicability of the MARS' derived equation is constrained by the used input ranges, which covers geometrical properties of the width of the steel tube, the depth of the steel tube, the length of the column, and the eccentricity were varied from 65 m to 323 mm, 47.3 m to 323 mm, 2.65 mm to 10.01 mm, 360 mm to 4910 mm, respectively, and material properties including up to 80.3 MPa of the concrete strength and 761 MPa of the yield strength of the steel. Consequently, for cases in which the input variable values are beyond this range, the proposed GS-MARS model should be used with caution.

5. Future work should validate the proposed explicit formulation by implementing it in a distinct database. It also should be noted that, like all empirical models, the range of applicability of the MARS derived formula is constrained by the data used in the model. To update the model and make it more robust in the future, it would be desirable to increase the number of data samples so that the model can be re-trained.

Acknowledgments

This research was supported by Ministry of Land, Infrastructure and Transport of Korean Government (Grant 20CTAP-C143093-03).

References

American Concrete Institute (ACI) (2011), Building Code Requirements for Structural Concrete and Commentary, ACI 318-11, Farmington Hills, MI, USA.

American Concrete Institute (ACI) (2014), Building Code Requirements for Structural Concrete and Commentary, ACI 318-14, Farmington Hills, MI, USA.

American Institute of Steel Construction (ANSI/AISC 360-10) (2010), Specification for Structural Steel Buildings, An American National Standard.

American Institute of Steel Construction (ANSI/AISC 360-10) (2016), Specification for Structural Steel Buildings, An American National Standard.

Ahmadi, M., Naderpour, H. and Kheyroddin, A. (2014), "Utilization of artificial neural networks to prediction of the capacity of CCFT short columns subject to short term axial load", *Arch. Civil Mech. Eng.*, **14**(3), 510-517. https://doi.org/10.1016/j.acme.2014.01.006.

Aslani, F., Uy, B., Tao, Z. and Mashiri, F. (2015), "Predicting the axial load capacity of high-strength concrete filled steel tubular columns", *Steel Compos. Struct.*, **19**(4), 967-993. https://doi.org/10.12989/scs.2015.19.4.967.

Bahrami, A., Hamidon, W. and Badaruzzaman, W. (2012), "Structural behaviour of tapered concrete-filled steel composite (TCFSC) columns subjected to eccentric loading", *Comput. Concrete*, **9**(6), 403-426. https://doi.org/10.12989/cac.2012.9.6.403.

Bradford, M.A., Loh, H.Y. and Uy, B. (2002), "Slenderness limits for filled circular steel tubes", *J. Constr. Steel Res.*, **58**(2), 243-252. https://doi.org/10.1016/S0143-974X(01)00043-8.

Bridge, R. (1976), "Concrete-filled steel tubular columns", Institution of Engineers, Australia.

Bui, D.K., Nguyen, T., Chou, J.S., Nguyen-Xuan, H. and Ngo, T.D. (2018), "A modified firefly algorithm-artificial neural network expert system for predicting compressive and tensile strength of high-performance concrete", *Constr. Build. Mater.*, **180**, 320-333. https://doi.org/10.1016/j.conbuildmat.2018.05.201.

Cheng, M.Y. and Cao, M.T. (2014), "Evolutionary multivariate adaptive regression splines for estimating shear strength in reinforced-concrete deep beams", *Eng. Appl. Artif. Intell.*, **28**, 86-96. https://doi.org/10.1016/j.engappai.2013.11.001.

Cheng, M.Y. and Cao, M.T. (2016), "Estimating strength of rubberized concrete using evolutionary multivariate adaptive regression splines", *J. Civil Eng. Manage.*, **22**(5), 711-720. https://doi.org/10.3846/13923730.2014.897989.

Craven, P. and Wahba, G. (1978), "Smoothing noisy data with spline functions", *Numer. Math.*, **31**(4), 377-403. https://doi.org/https://doi.org/10.1007/BF01404567.

Dutta, S., Samui, P. and Kim, D. (2018), "Comparison of machine learning techniques to predict compressive strength of concrete", *Comput. Concrete*, **21**(4), 407-417. https://doi.org/10.12989/cac.2018.21.4.463.

Friedman, J.H. (1991), "Multivariate adaptive regression splines", *Ann. Statics*, **19**(1), 1-67.

Fujimoto, T., Mukai, A., Nishiyama, I. and Sakino, K. (2004), "Behavior of eccentrically loaded concrete-filled steel tubular columns", *J. Struct. Eng.*, **130**(2), 203-212. https://doi.org/10.1061/(ASCE)0733-9445(2004)130:2(203).

Ghasemian, M. and Schmidt, L.C. (1999), "Curved Circular Hollow Section (CHS) Steel Struts Infilled with Higher-Strength Concrete", *Struct. J.*, **96**(2), 275-281. https://doi.org/10.14359/619.

Güneyisi, E.M., Gültekin, A. and Mermerdaş, K. (2016), "Ultimate capacity prediction of axially loaded CFST short columns", *Int. J. Steel Struct.*, **16**(1), 99-114. https://doi.org/10.1007/s13296-016-3009-9.

Guo, L.H., Zhang, S.M. and Tian, H. (2004), "High strength concrete-filled RHS steel tubes subjected to eccentric loading", *Harbin Gongye Daxue Xuebao/J. Harbin Inst. Technol.*, **36**(3), 297-301.

Gupta, P.K., Verma, V.K., Khaudhair, Z.A. and Singh, H. (2015), "Effect of tube area on the behavior of concrete filled tubular columns", *Comput. Concrete*, **15**(2), 141-166. https://doi.org/10.12989/cac.2015.15.2.141.

Han, B., Wang, Y., Wang, Q. and Zhang, D. (2013), "Creep analysis of CFT columns subjected to eccentric compression loads", *Comput. Concrete*, **11**(4), 291-304. https://doi.org/10.12989/cac.2013.11.4.291.

Han, L.H.H., Li, W. and Bjorhovde, R. (2014), "Developments and advanced applications of concrete-filled steel tubular (CFST) structures: Members", *J. Constr. Steel Res.*, **100**, 211-228. https://doi.org/10.1016/j.jcsr.2014.04.016.

Han, L.H. and Yao, G.H. (2003), "Influence of concrete compaction on the strength of concrete-filled steel RHS columns", *J. Constr. Steel Res.*, **59**(6), 751-767.

https://doi.org/10.1016/S0143-974X(02)00076-7.

Ipek, S. and Güneyisi, E.M. (2019), "Ultimate axial strength of concrete-filled double skin steel tubular column sections", *Adv. Civil Eng.*, **2019**. https://doi.org/10.1155/2019/6493037.

Knowles, R. and Park, R. (1970), "Axial load design for concrete filled steel tubes", *J. Struct. Div.*, **96**(12), 2125-2153.

Knowles, R. and Park, R. (1969), "Strength of concrete filled steel tubular columns", *J. Strucural Div.*, **95**(12), 2565-2587.

Kuranovas, A., Goode, D., Kvedaras, A.K. and Zhong, S. (2009), "Load-bearing capacity of concrete-filled steel columns", *J. Civil Eng. Manage.*, **15**(1), 21-33. https://doi.org/10.3846/1392-3730.2009.15.21-33.

Lee, S.H., Uy, B., Kim, S.H., Choi, Y.H. and Choi, S.M. (2011), "Behavior of high-strength circular concrete-filled steel tubular (CFST) column under eccentric loading", *J. Constr. Steel Res.*, **67**(1), 1-13. https://doi.org/10.1016/j.jcsr.2010.07.003.

Liu, D. (2004), "Behaviour of high strength rectangular concrete-filled steel hollow section columns under eccentric loading", *Thin Wall. Struct.*, **42**(12), 1631-1644. https://doi.org/10.1016/j.tws.2004.06.002.

Liu, J., Wang, X., Qi, H. and Zhang, S. (2015), "Behavior and strength of circular tubed steel- reinforced-concrete short columns under eccentric loading", *Adv. Struct. Eng.*, **18**(10), 1587-1595. https://doi.org/10.1260/1369-4332.18.10.1587.

Lu, Z.H. and Zhao, Y.G. (2010), "Suggested empirical models for the axial capacity of circular CFT stub columns", *J. Constr. Steel Res.*, **66**(6), 850-862. https://doi.org/10.1016/j.jcsr.2009.12.014.

Mursi, M. (2007), "The behaviour and design of thin walled concrete filled steel box columns", Ph. D. Thesis, School of Civil and Environmental Engineering, The University of New South Wales.

Nakahara, H. and Sakino, K. (2000), "Practical analysis for high-strength CFT columns under eccentric compression", *Composite and Hybrid Structures : Proceedings of the 6th ASCCS International Conference on Steel-Concrete Composite Structures*, Univ. of Southern California, Los Angeles, CA.

Neogi, P., San, H. and Chapman, J. (1969), "Concrete filled tubular steel columns uncer eccentric loading", *J. Struct. Eng.*, **47**(5), 187-195.

Pedregosa, F., Varoquaux, G., Gramfort, A., Michel, V., Thirion, B., Grisel, O., ... & Vanderplas, J. (2011), "Scikit-learn: Machine learning in python", *J. Mach. Learn. Res.*, **12**, 2825-2830.

Portolés, J.M., Romero, M.L., Bonet, J.L. and Filippou, F.C. (2011), "Experimental study of high strength concrete-filled circular tubular columns under eccentric loading", *J. Constr. Steel Res.*, **67**(4), 623-633. https://doi.org/10.1016/j.jcsr.2010.11.017.

Qi, C. and Tang, X. (2018), "A hybrid ensemble method for improved prediction of slope stability", *Int. J. Numer. Anal. Meth. Geomech.*, **42**(15), 1823-1839. https://doi.org/10.1002/nag.2834.

Rangan, B.V. and Joyce, M. (1992), "Strength of eccentrically loaded slender steel tubular columns filled with high-strength concrete", *ACI Struct. J.*, **89**(6), 676-681.

Ren, Q., Li, M., Zhang, M., Shen, Y. and Si, W. (2019), "Prediction of ultimate axial capacity of square concrete-filled steel tubular short columns using a hybrid intelligent algorithm", *Appl. Sci.*, **9**(14). https://doi.org/10.3390/app9142802.

Saadoon, A.S., Nasser, K.Z. and Mohamed, I.Q. (2012), "A neural network model to predict ultimate strength of rectangular concrete filled steel tube beam-columns", *Eng. Technol. J.*, **30**(19), 3328-3340.

Schneider, S.P. (1998), "Axially loaded concrete-filled steel tubes", *J. Struct. Eng.*, **124**(10), 1125-1138. https://doi.org/10.1061/(ASCE)0733-9445(1998)124:10(1125).

Shakir-Khalil, H. and Al-Rawdan, A. (1996), "Experimental behaviour and numerical modelling of concrete-filled rectangular hollow section tubular columns", *Proceedings of an Engineering Foundation Conference*, Irsee, Germany, 222-235.

Shakir-Khalil, H. and Zeghiche, J. (1989), "Experimental behaviour of concrete-filled rolled rectangular hollow-section columns", *Struct. Eng.*, **67**(19), 346-353.

Tao, Z., Uy, B., Han, L.H. and He, S.H. (2008), "Design of concrete-filled steel tubular members according to the Australian Standard AS 5100 model and calibration", *Aust. J. Struct. Eng.*, **8**(3), 197-214. https://doi.org/10.1080/13287982.2008.11464998.

Tomii, M., Yoshimura, K. and Morishita, Y. (1977), "Experimental studies on concrete filled steel tubuar stub columns under concentric loading", *International Colloquium on Stability of Structures Under Static and Dynamic Loads*. Washington, D.C, United States.

Uy, B. and Das, S. (1997), "Behaviour and design of concrete filled fabricated steel box columns", *Proceedings of 15th Australasian Conference on the Mechanics of Structures and Materials*, Melbourne, Australia.

Uy, B., Tao, Z. and Han, L.H. (2011), "Behaviour of short and slender concrete-filled stainless steel tubular columns", *J. Constr. Steel Res.*, **67**(3), 360-378. https://doi.org/10.1016/j.jcsr.2010.10.004.

Vrcelj, Z. and Uy, B. (2002), "Behaviour and design of steel square hollow sections filled with high strength concrete", *Aust. J. Struct.*, **3**(3), 153-170. https://doi.org/10.1080/13287982.2002.11464902.

Wei, Z. and Han, L. (2000), "Research on the bearing capacity of early-strength concrete filled square steel tube", *Composite and Hybrid Structures: Proceedings of the 6th ASCCS International Conference on Steel-Concrete Composite Structures*, Univ. of Southern California, Los Angeles, CA.

Zeghiche, J. and Chaoui, K. (2005), "An experimental behaviour of concrete-filled steel tubular columns", *J. Constr. Steel Res.*, **61**(1), 53-66. https://doi.org/10.1016/j.jcsr.2004.06.006.

Zhang, S. and Guo, L. (2007), "Behaviour of high strength concrete-filled slender RHS steel tubes", *Adv. Struct. Eng.*, **10**(4), 337-351. https://doi.org/10.1260/136943307783239381.

Zhang, W. and Goh, A.T.C. (2015), "Nonlinear structural modeling using multivariate adaptive regression splines", *Comput. Concrete* **16**(4), 569-585. https://doi.org/10.12989/cac.2015.16.4.569.

Zhu, W.C., Ling, L., Tang, C.A., Kang, Y.M. and Xie, L.M. (2012), "The 3D-numerical simulation on failure process of concrete-filled tubular (CFT) stub columns under uniaxial compression", *Comput. Concrete*, **9**(4), 257-273. https://doi.org/10.12989/cac.2012.9.4.257

CC

Appendix

Experimental data of CFST columns under axial load used in the MARS model

References	No.	B (mm)	H (mm)	t (mm)	L (mm)	f_{sy} (MPa)	f'_c (MPa)	e (mm)	N_u (kN)
Nakahara and Sakino (2000)	1	149	149	4.4	447	262	41.1	45	755
	2	149	149	4.4	447	262	41.1	200	259
	3	216	216	4.4	648	262	25.4	60	1141
	4	216	216	4.4	648	262	25.4	200	503
	5	216	216	6.4	648	262	41.1	100	1028
	6	215	215	6.4	645	262	41.1	200	580
	7	216	216	6.4	648	262	80.3	60	2013
	8	216	216	6.4	648	262	80.3	100	1447
	9	323	323	6.4	969	262	41.1	60	3306
	10	323	323	6.4	969	262	41.1	200	1479
	11	145	145	6.4	435	618	41.1	45	1636
	12	145	145	6.4	435	618	41.1	200	611
	13	211	211	6.4	633	618	25.4	60	2393
	14	211	211	6.4	633	618	41.1	60	2685
	15	211	211	3.0	633	618	41.1	100	2090
	16	212	212	3.0	636	618	41.1	300	858
	17	211	211	3.0	633	618	80.3	60	3396
	18	211	211	3.0	633	618	80.3	200	1484
	19	318	318	3.0	954	618	41.1	100	4100
	20	319	319	3.0	957	618	41.1	300	1967
	21	216	216	4.4	648	262	68.26	60	2013
	22	216	216	4.4	648	262	68.26	100	1447
	23	211	211	6.4	633	618	68.26	60	3396
	24	211	211	6.4	633	618	68.26	200	1484
Uy and Das (1997)	25	186	186	4.4	540	300	32	37	1069
	26	186	186	4.4	540	300	32	56	1133
	27	186	186	4.4	540	300	32	84	895
	28	126	126	4.4	360	300	50	20	996
	29	126	126	4.4	360	300	50	40	739
	30	126	126	6.4	360	300	50	50	619
Shakir-Khalil and Al-Rawdan (1996)	31	100	150	5.0	2940	330.8	36.08	6	882
	32	100	150	5.0	2940	331.5	37.76	15	670
	33	100	150	5.0	2940	331.5	38.48	45	470
	34	100	150	5.0	2940	321.6	37.92	75	339
	35	100	150	5.0	4000	360.8	37.6	6	667
	36	100	150	5.0	4000	355.5	38.16	15	650
	37	100	150	5.0	4000	350.5	38.64	45	443
	38	100	150	5.0	4000	342.5	38.56	75	344
	39	100	150	5.0	4910	360.8	36.56	6	536
	40	100	150	5.0	4910	342.5	37.04	15	558
	41	100	150	5.0	4910	368	37.84	45	356
	42	100	150	5.0	2940	324.3	41.2	30	402
	43	100	150	5.0	4000	368	36.56	30	349
	44	100	150	5.0	4910	355.5	37.76	30	273
Wei and Han (2000)	45	120	120	3.8	2600	330.1	15.144	15	588
	46	120	120	3.8	2600	330.1	15.144	30	450.8
	47	120	120	3.8	2600	330.1	20.368	40	421.4
	48	120	120	3.8	2600	330.1	15.144	50	333.2
	49	120	120	3.8	2600	330.1	20.368	40	417.5
	50	120	120	3.8	2600	330.1	29.28	50	423.4
	51	140	140	3.8	2600	330.1	18.84	15	833
	52	140	140	3.8	2600	330.1	18.84	40	615.4
	53	140	140	3.8	2600	330.1	18.84	60	509.6
	54	140	140	3.8	2600	330.1	20.368	40	558.6
	55	140	140	3.8	2600	330.1	29.28	60	539
	56	120	120	5.9	2600	321.1	18.84	15	754.6
	57	120	120	5.9	2600	321.1	18.84	30	548.8

Continued

References	No.	B (mm)	H (mm)	t (mm)	L (mm)	f_{sy} (MPa)	f'_c (MPa)	e (mm)	N_u (kN)
Wei and Han (2000)	58	120	120	5.9	2600	321.1	18.84	50	510.6
	59	140	140	5.9	2600	321.1	15.376	15	1014.3
	60	140	140	5.9	2600	321.1	15.376	30	803.6
	61	140	140	5.9	2600	321.1	15.008	40	735
	62	140	140	5.9	2600	321.1	15.008	60	555.7
	63	200	200	5.9	2600	321.1	21.416	80	1200.5
Han and Yao (2003)	64	130	195	2.7	780	340	18.46	14	872
	65	130	195	2.7	780	340	18.46	14	812
	66	130	195	2.7	780	340	18.46	31	646
	67	130	195	2.7	780	340	18.46	31	610
	68	130	195	2.7	2340	340	18.46	14	670
	69	130	195	2.7	2340	340	18.46	14	635
Zhang and Guo (2007)	70	150.2	150.2	2.9	1110	319.3	68.5	1.1	2352
	71	149.5	149.5	2.9	2200	319.3	68.5	3.5	2077
	72	148.6	148.6	2.9	3101	319.3	68.5	2.5	1558
	73	151.4	151.4	4.8	1085	316.6	68.5	1.1	2597
	74	150	150	4.9	2201	316.6	68.5	2	2381
	75	150.7	150.7	4.9	3100	316.6	68.5	3.5	1627
	76	134.9	175.7	2.9	993	319.3	68.5	1	2401
	77	136.3	176.5	2.9	1980	319.3	68.5	3	2283
	78	124.6	199.3	2.9	921	319.3	68.5	0.9	2636
	79	125.9	199.9	2.9	1829	319.3	68.5	1.5	2303
	80	149.4	149.4	2.9	1090	319.3	68.5	43	1147
	81	150.4	150.4	2.9	1115	319.3	68.5	22	1597
	82	149.8	149.8	2.9	2203	319.3	68.5	23.5	1274
	83	148.3	148.3	2.9	3101	319.3	68.5	26	941
	84	152.1	152.1	4.8	1105	316.6	68.5	41.5	1416
	85	150.6	150.6	4.9	1100	316.6	68.5	21.1	1901
	86	150.8	150.8	4.9	2199	316.6	68.5	21	1519
	87	150.4	150.4	4.9	3100	316.6	68.5	25.5	1103
	88	135.7	176.2	2.9	988	319.3	68.5	20.5	1911
	89	134.1	173.5	2.9	989	319.3	68.5	41	1343
	90	134.8	174.9	2.9	988	319.3	68.5	72	823
	91	136.4	174.6	2.9	1982	319.3	68.5	21	1588
	92	137.2	176.2	4.8	990	316.6	68.5	20	2058
	93	137.2	175.1	4.8	1980	316.6	68.5	22	1813
	94	125	200.5	2.9	919	319.3	68.5	41	1529
	95	125.1	201.4	2.9	1831	319.3	68.5	38	1548
Guo *et al.* (2004)	96	100.5	200.7	3.6	1800	283.6	41.8	40	1002.3
	97	149	149	3.6	450	283.6	41.8	30	1081.9
	98	99.1	200	3.7	600	283.6	41.8	40	1036.8
	99	80	120	5.0	3120	386.3	37.4	24	393
	100	80	120	5.0	3121	386.3	37.4	60	232
Liu (2004)	101	150	150	4.2	870	550	56.64	30	1678
	102	150	150	4.2	870	550	65.68	30	1850
	103	150	150	4.2	2170	550	56.64	30	1330
	104	150	150	4.2	2170	550	65.68	60	1020
	105	120	180	4.2	1040	550	56.64	30	1950
	106	120	180	4.2	1040	550	65.68	70	1140
	107	80	120	4.2	1740	550	56.64	20	660
	108	80	120	4.2	1740	550	65.68	20	855
	109	100	200	4.2	1150	550	56.64	60	1310
	110	100	200	4.2	1150	550	65.68	40	1800
	111	80	160	4.2	2310	550	56.64	60	670
	112	80	160	4.2	2310	550	65.68	30	1020
Bridge (1976)	113	203.7	203.9	10.0	2130	291	30.2	39.	1956
	114	203.3	204	10.0	3050	290	30.6	1.4	2869
	115	152.3	152.3	6.5	3050	254	35	38.51	680
	116	152.3	152.3	6.5	3051	254	35	65.02	513

Continued

References	No.	B (mm)	H (mm)	t (mm)	L (mm)	f_{sy} (MPa)	f'_c (MPa)	e (mm)	N_u (kN)
Vrcelj and Uy (2002)	117	75	75	3.0	1770	370	78.6	3.75	414
	118	65	65	3.0	1770	350	78.6	3.25	294
	119	75	75	3.0	1770	370	51.8	3.75	343
	120	65	65	3.0	1770	350	51.8	3.25	269
Mursi (2007)	121	110	110	5.0	3020	761	20.34	10	1036
	122	160	160	5.0	3020	761	20.34	15	1505
	123	260	260	5.0	3020	761	20.34	25	1371
	124	120	120	5.0	460	754.2	20.27	10	1395
	125	220	220	5.0	730	754.2	20.27	20	1421
	126	270	270	5.0	880	754.2	20.27	25	1471
	127	120	120	5.0	431	754.2	20.27	10	1609
	128	203.7	203.9	10.0	2130	291	30.2	39.19	1952
	129	203.3	204	10.0	3050	290	30.6	1.4	2993
	130	152.3	152.3	6.5	3050	254	35	38.51	708
	131	152.3	152.3	6.5	3051	254	35	65.02	543
	132	80	120	5.0	3120	386.3	37.4	24	405.6
	133	80	120	5.0	3121	386.3	37.4	60	233
	134	75	75	3.0	1770	370	78.6	3.75	390.3
	135	65	65	3.0	1770	350	78.6	3.25	269.4
	136	75	75	3.0	1770	370	51.8	3.75	338
	137	65	65	3.0	1770	350	51.8	3.25	255
	138	120	120	5.0	3020	761	20.34	8	1481
	139	170	170	5.0	3020	761	20.34	15	2126
	140	220	220	5.0	3020	761	20.34	18	2939
	141	270	270	5.0	3020	761	20.34	23	3062